Motile Artificial Chromatophores: Light-Triggered Nanoparticles for Microdroplet Locomotion and Color Change

*Andrew R Salmon, Sean Cormier, Wenting Wang, Chris Abell, and Jeremy J Baumberg**

Dr A. R. Salmon[†], S. Cormier[†], W. Wang, Prof. J. J. Baumberg
Nanophotonics Centre, Cavendish Laboratory, University of Cambridge, CB3 0HE, United Kingdom

Prof. C. Abell
Department of Chemistry, University of Cambridge, CB2 1EW, United Kingdom

E-mail: jjb12@cam.ac.uk

Keywords: microswimmers, chromatophores, poly(N-isopropylacrylamide), biomimetics, microdroplets

Gold nanoparticles coated with a poly(N-isopropylacrylamide) (pNIPAM) shell undergo reversible dis/assembly below and above the critical temperature of 32°C. Loading these particles into microdroplets at high density creates light-driven artificial chromatophores. Triggering the nanoparticle assembly gives dramatic color changes from nanoparticle localization at the base of the droplets, resembling zebrafish melanophores. These reversible chromatophore states can be switched by both bulk and optical heating, explored here in individual microdroplets and in large cm^2 areas of close-packed droplets. Illuminating chromatophores off-center with a tightly focused beam results in droplet locomotion via two separate mechanisms, Marangoni interfacial shear and gas bubble propulsion, depending on optical power.

Motor proteins, such as myosin and kinesin, move functional components within cells. In chromatophore cells, these molecular machines are used to reversibly manipulate pigments and nanocrystals to give strong changes in color and transparency. Chromatophores are used for active camouflage in a wide range of animals, including cuttlefish, zebrafish and chameleons.[1–3] There is increasing interest in mimicking such behavior for diverse applications from dynamic color displays to artificial active camouflage.[4–7] Developing biomimetic locomotion at the micro- and nanoscale is a correspondingly active research theme.[8–10] Light-driven locomotion is especially promising because it allows for simple remote control without electrical wiring compromising motion, as well as high spatial and temporal resolution.[11,12] In biomimicry of both chromatophores and cell locomotion, artificial systems must be developed that can use nanoscale actuation to produce effects on the microscale.

Recently it was demonstrated that gold nanoparticles (NPs) can be reversibly dis/assembled with light using a poly(N-isopropylacrylamide) (pNIPAM) shell.[13,14] The pNIPAM undergoes a lower critical solution temperature (LCST) phase change at T_c=32°C between a hydrated and dehydrated state. Above 32°C the pNIPAM shell shrinks as water is expelled and the coating increases in hydrophobicity. The particles then agglomerate due to strong interparticle cohesion forces. When the temperature is cooled below 32°C the pNIPAM

[†] Equal contributions from these authors

rapidly swells, forcing the agglomerated particles to separate. The relatively large optical absorption cross-section of small Au NPs allows efficient local heating above the LCST with focused light. These Au@pNIPAM core-shell nanoparticles thus provide a promising platform to exploit the mechanical work done during the phase change of pNIPAM with light. Other authors have also shown the potential of Au@pNIPAM core-shell nanoparticles as sensors.[15,16]

Here we show that light-responsive artificial chromatophores can be created by loading microdroplets with Au@pNIPAM nanoparticles. The microdroplets both limit the size of the nanoparticle clusters and can localize them to the oil-water interface. This results in dramatic color changes during few °C heating and cooling, and highly repeatable cycling. Intriguingly, the preferential assembly of nanoparticle clusters at the oil-water interface generates locomotion, shown to arise through two separate mechanisms. Under strong laser illumination, high pressure microbubbles are rapidly formed at the interface that expand and ballistically propel the droplets on ms timescales. Under weaker illumination, the localization of NPs to the liquid interface increases the local surface tension and creates a gradient across the microdroplet that drives Marangoni flows. This results in interfacial shear which causes droplets to swim. This significant advance in artificial nanoscale actuation delivers microscale function, analogous to the pervasive use of nanoscale motor proteins in biology.

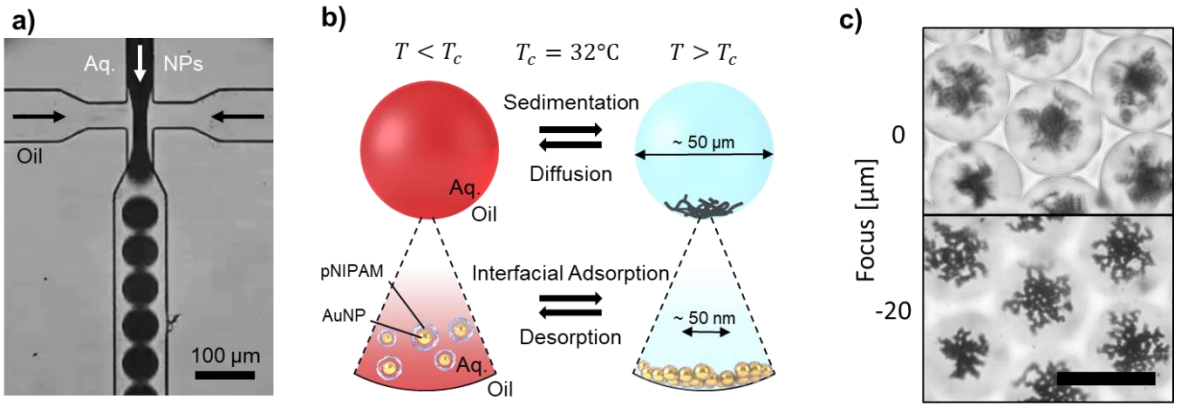

Figure 1. Au@pNIPAM core-shell nanoparticles (10^{14} ml^{-1}) in water-in-oil microdroplets for artificial chromatophores. a) Optical micrograph of the formation of chromatophore microdroplets at a flow-focusing microfluidic junction. b) Schematic temperature response of the chromatophore microdroplets. c) Optical microscopy transmission images of aggregated 'hot' state at different focal heights (high NA objective). Clusters sediment to bottom of droplets, scale bar is 50 µm.

Au@pNIPAM core-shell nanoparticles are made by ligand exchange as previously reported,[13] but here substantially higher particle concentrations are used enabling us to enhance thermo-optic and opto-fluidic coupling. In order to achieve this, relatively dense 14 nm citrate-capped AuNPs are first synthesized (see methods). The citrate capping ligands are next exchanged for 5.5 kDa amine-terminated pNIPAM. The resulting Au@pNIPAM core-shell nanoparticles are then concentrated by a factor of 10 by centrifugation to give a final concentration of 10^{14} ml^{-1}. Although citrate-capped particles are found to aggregate at this concentration, the steric stabilization provided by the pNIPAM here (below T_c) is sufficient to prevent this.

The Au@pNIPAM core-shell nanoparticles are then loaded into microdroplets using a flow-focusing microfluidic device and a fluorocarbon oil phase (**Figure 1**a). The droplet generation rate is approximately 1000 s^{-1}. The droplets are transferred to a sealed liquid cell, which allows for further analysis without their evaporation. The Au@pNIPAM core-shell nanoparticles reversibly aggregate and disaggregate above and below the critical solution temperature (**Figure 1**b).

As a result of the decreased hydrophilicity, above T_c the particles preferentially adsorb onto the oil-water interface of the microdroplets. By confocal microscopy, the 'hot' Au@pNIPAM NPs are then observed to assemble in 2D fractal structures (**Figure 1**c), characteristic of diffusion limited aggregation.[17] The assemblies sediment to the base of the droplets as a result of their larger size and dense Au NP composition. However, unlike bulk sedimentation, the droplet encapsulation limits both the aggregate size and the length scale over which the particles sediment. From the nanoparticle concentration and the droplet volume, the number of nanoparticles per droplet is ~10^6. Since this is equivalent to a 1.4 μm diameter Au sphere, the large aggregate fractal areas are evidently extremely thin. Further multi-scale assembly processes must also operate to construct the fractal arms of ~5 μm width (**Figure 1**c). The implication is that initially micron-scale clusters form, and then these in turn cluster to form the observed structures. Upon cooling the droplets below T_c, the sedimented NPs quickly disaggregate from the >nN pNIPAM expansion forces and redisperse throughout the droplet under Brownian forces.[13] Crucially, this process is fully reversible over repeated heating and cooling cycles.

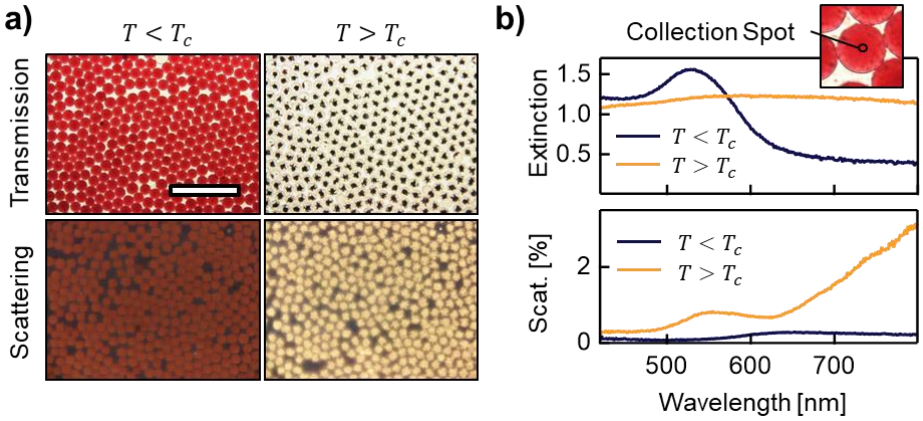

Figure 2. Reversible temperature-induced optical response of the microdroplet chromatophores. a) Microscope images acquired in bright field transmission mode (top images) and dark field incident illumination mode (bottom images) at temperatures below and above the critical temperature T_c = 32°C). Scale bar is 200 μm. b) Extinction and scattering spectra below and above T_c acquired from a 2 μm spot in the center of the droplets shown highlighted in the top-right inset.

The optical properties of each droplet are strongly dependent on the internal distribution of NPs. The transmission and scattering of droplets thus change drastically with temperature. (**Figure 2**). In transmission, their color changes from red to predominantly transparent with a strong black center. For dark-field scattering however (light incident at 5° and collected at normal incidence), they become much brighter in the hot aggregated state while also changing color. This is caused by large changes in scattering cross-section brought on by plasmonic coupling

between the closely packed Au NPs. These changes are evident in the spectra, taken from a 2 µm collection region at the center of the droplets **(Figure 2**b). The Au NP plasmon mode at 526 nm is seen to redshift into infrared chain plasmons in the assembled state.[18] As the Au NP cores approach more closely, the plasmonic modes couple to produce the broad extinction across the spectral range. The scattering also strongly increases because aggregates have a higher scattering cross-section than the sum of the monomers they are composed of. The high NP concentrations used produce extinctions across each single 50 µm droplet comparable to that of standard nanoparticle solutions through 1 cm path-lengths. Notably the extinction in the assembled state covers the whole visible spectrum, whereas the Au@pNIPAM monomers absorb predominantly blue/green light.

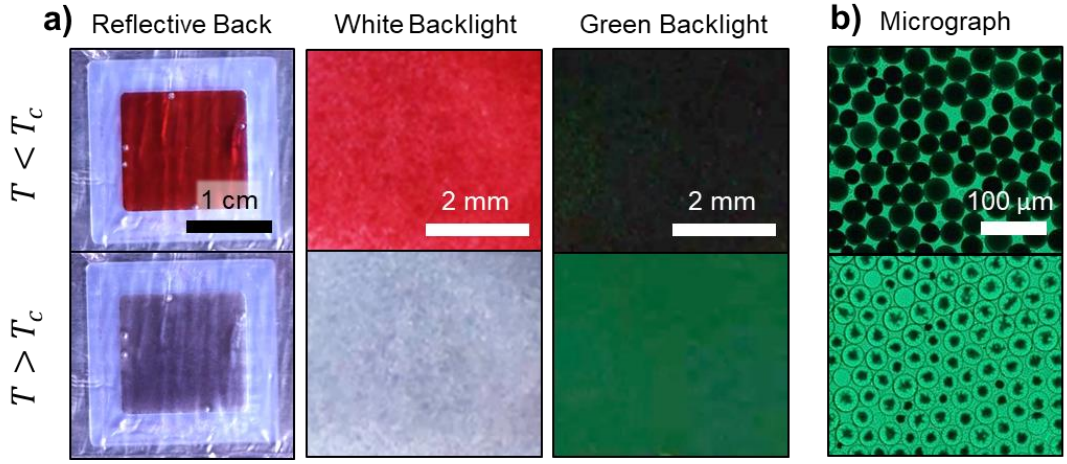

Figure 3. a) Camera images showing large area switching of the microdroplet chromatophores with temperature (T_c = 32˚C) in various lighting conditions. b) Optical transmission micrograph of the microdroplet chromatophores with a green backlight.

Using this optical switch, we are able to make active chromatophore layers over large areas (**Figure 3**). These are assembled by simply loading a liquid cell with the chromatophore droplets and the oil continuous phase. The droplets float on the oil and geometrically pack. With a white or reflective backing, their colors transition between the red of the Au@pNIPAM monomers and a transparent grey. Highest transmission contrast is achieved using a green backlight, which is strongly absorbed by the Au@pNIPAM monomers. In this case the transmission decreases by ~50% below T_c. The on/off half-cycle switch time is ~5 s (video, supporting information), which matches timescales considered rapid for biological chromatophores.[2] Similar switching rates are obtained with rapid laser heating, indicating that the transition time is limited by the Au NP aggregation process rather than heat transfer rates. The transition can thus be accelerated using smaller droplets to decrease the sedimentation distance, with the trade-off of reduced pathlength decreasing the extinction.

The drastic contrast in transmission in response to slight changes in temperature is caused by the localization of the absorbing Au@pNIPAM particles at the center of the droplets above T_c (**Figure 3**b). This allows for enhanced transmission of light through the droplet periphery. Because light attenuation is non-linear with concentration (nanoparticles shadow each other) this enhanced transmission through the periphery outweighs the decreased transmission through the center. This is the same mechanism by which many pigment-based

chromatophores operate, such as the melanophores in zebrafish.[19] To the best of our knowledge, this is the first replication of this mechanism in a fully artificial system.

In biological systems different colored chromatophores will often be used in combination for enhanced effect. We have previously shown reversible assembly of other nanostructures such as silver nanoparticles,[13] and it is well known that the LCST of pNIPAM can be tuned (or pH responsive polymers can be used). Consequently, future development of multi-colored chromatophore layers which independently switch is now feasible. Similarly, transparent microwells could be used instead of droplets to create fixed chromatophore arrays.

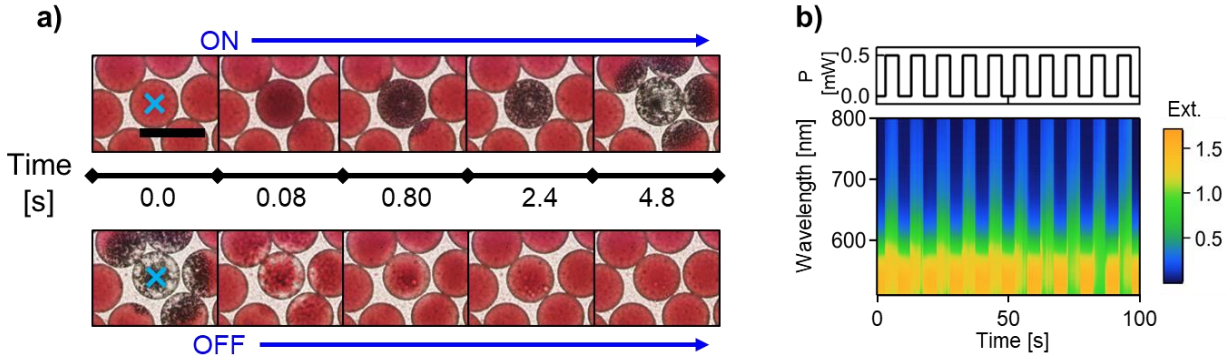

Figure 4. Switching the microdroplet chromatophores with light using a 447 nm beam centered on the microdroplet. The images are acquired through a 500 nm long pass filter to remove laser scatter. a) Transmission video frames when switching the laser on and off. The scale bar is 50 µm. The blue crosses mark the 2 µm laser spot positions. b) Time series spectra map with the irradiation cycled at 100 mHz (50% duty cycle).

Next we investigate locally heating the microdroplet chromatophores using laser illumination at 447 nm. In this spectral region the gold interband transition results in strong absorption. Centering the laser spot on a droplet, 0.5 mW (0.16 mW µm^{-2}) produces observable color changes on millisecond timescales. The heat from the illuminated volume conducts throughout the droplet and through the continuous oil phase to neighboring droplets (fluorocarbon oils have excellent heat transfer properties and are often used for cooling electronics).[20] Time resolved spectra demonstrate that this is fully reversible and repeatable (**Figure 4**b). The well-defined boundaries observed between monomer/aggregated regions (0.80s and 4.8s in **Figure 4**a) resolve the sharp pNIPAM transition at T_c within the thermal gradient. The short timescales involved in the assembly can be explained by the high particle concentrations. Aggregation of nanoparticles within microdroplets is well described by the diffusion-limited colloidal aggregation model in which the characteristic aggregation timescale is inversely proportional to concentration.[21]

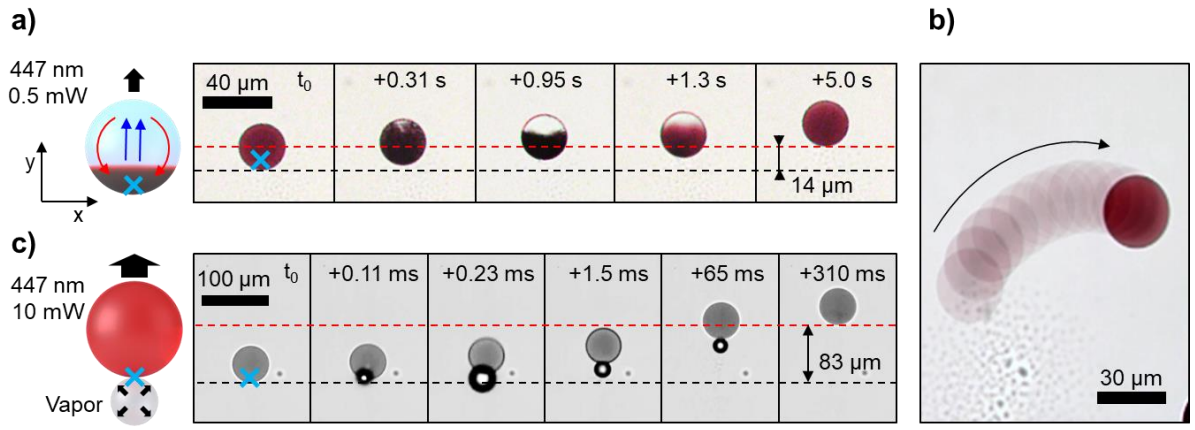

Figure 5. Off-center irradiation for microdroplet chromatophore locomotion, showing Marangoni flow and gas expansion propulsion mechanisms. a) Schematic of Marangoni flow induced swimming by off-center laser-induced heating, with time-stamped microscope video frames. b) Superimposed sequential images showing locomotion over repeated illumination cycles. c) Schematic of gas expansion mechanism for locomotion, with time-stamped microscope video frames taken with a high-speed camera. Black and red dashed lines mark start and stop positions of the microdroplets, respectively. Blue cross marks 2 µm laser spot position.

It has been noted that the Au@pNIPAM clusters localize to the droplet interface. Consequently, effects on the interfacial tension are anticipated and these could drive droplet motion. However, with either bulk heating or centered laser irradiation the clusters localize to the bottom interface. This mean that any forces generated either compete with the strong buoyant forces or push into the wall of the liquid cell. Remarkably, if instead the laser focus is off-center, irradiation results in locomotion of the microdroplet chromatophores (**Figure 5**a). The high contrast of the active nanoparticles enables us to establish the mechanism. First, illumination locally heats the Au@pNIPAM NPs generating a temperature gradient across the droplet. The temperature-switched NPs have reduced hydrophilicity causing them to localize to the interface. pNIPAM colloids are known to increase surface tension at the oil-water interface for temperatures just above T_c due to increased interparticle cohesion.[22,23] With the temperature gradient, this preferentially increases the surface tension on the illuminated side of the droplet and causes Marangoni flow at the interface (**Figure 5**a). The interfacial flow results in a shear force that propels the droplet.

The condition for locomotion at low Reynold's number (in Newtonian fluids) is that the swimming action is non-reciprocal with time.[24] Consequently, if the interfacial flow simply reversed once the droplet was out of the laser spot then the drop would return to its starting position. Instead, after the propulsion the particles diffuse away from the interface and consequently break the symmetry. Overall the swimming action can be summarized as Marangoni interfacial propulsion followed by a diffusive recovery. In between each cycle the droplet is outside of the laser spot and so is stationary.

This optically-induced swimming of droplets by Marangoni flow has been previously well studied for chemical fuels.[25] The motion is termed 'squirming', after the similar swimming action used by microorganisms including *paramecium* and *volvox*. The key parameter that determines the locomotion velocity is the capillary number,

$$\mathrm{Ca} = \frac{\eta_s v}{\gamma} \approx \frac{2}{5}\frac{\Delta\gamma}{\gamma}$$

where η_s is the viscosity, v is the velocity and γ is the surface tension. The result is that the velocity is determined by the change in surface tension across the droplet. $\Delta\gamma$ is small relative to γ as the droplets remain spherical, but nevertheless sufficient to drive the droplets at microns per second.

At relatively high laser powers (2 mW, 0.6 mW μm^{-2} threshold) a different mode of chromatophore locomotion operates (**Figure 5**b). Locally high temperatures cause the generation of a gas bubble at high pressure. This bubble expands and propels the chromatophore before collapsing. In this case the movement is inertial: the bubble expansion and collapse is geometrically reciprocal yet net motion still occurs. The motion is fast enough that despite the high viscous damping there is still significant displacement.

There are three possible gas sources in the system: water vapor, oil vapor, and gas dissolved in the oil. Oil vapor can be ruled out as the boiling point of the oil (NOVEC 7500 fluorocarbon) is above that of water at 128°C. Water vapor formation is possible, however during the bubble collapse droplets of condensation would be expected in the oil. Additionally, we have not previously seen water vapor formation in the laser illumination of wet Au@pNIPAM particles.[26] Consequently, release of gas from the oil is the most likely candidate, in agreement with the lack of any size change of the microdroplet. Fluorocarbon oils are well known to hold large quantities of dissolved gas (~50% by volume).[27] The gas solubility decreases with temperature and thus bubbles form when the oil is heated. This is consistent with the observation that in some cases after formation the bubbles grow spontaneously, implying a nucleation event in a supersaturated solution.

Extracting from sequential video frames, we obtain peak velocities of 10 μm s^{-1} for the Marangoni mechanism and 92 mm s^{-1} for the gas propulsion mechanism.

In conclusion, we show that individual microdroplets densely loaded with Au@pNIPAM core-shell nanoparticles support functional behaviors from their actuation by heat or light which is entirely reversible. Chromatophore operation is demonstrated over large areas. Below T_c the plasmon resonance of the Au@pNIPAM individual NPs dictates the color while above T_c the nanoparticles agglomerate causing a dramatic increase in the chromatophore transparency. This precisely mimics the operation of pigment-based chromatophores. Optical switching of the chromatophores is achieved at sub-mW laser powers with high reversibility. Most significantly, off-center illumination of the artificial chromatophores results in droplet locomotion by two distinct mechanisms, droplet squirming and bubble-induced propulsion.

This represents a substantial advance in use of artificial nano-actuation to deliver microscale biomimicry. Following this development further optimization is now possible. For example, rapid refocusing of the laser spot at different locations can track the moving microdroplets, and thus create fully programmable movements of multiple chromatophores. This will open up new opportunities in active matter, as well as color-responsive fluidics. In addition, the aggregation can be photochemically triggered, thus potentially providing sensing functionalities for biofluidics devices.

Experimental Section

Au@pNIPAM core-shell nanoparticles

Concentrated 14 nm AuNPs were made following a modified Turkevich method.[28] A 200 ml aqueous solution 2.5 mM in $HAuCl_4$ and 7.7 mM in NaOH was prepared. This solution was heated to 85°C under reflux and then trisodium citrate was injected to a final concentration of 5 mM. After 20 minutes the resulting AuNP suspension was allowed to cool. The particles were measured to be 14±1 nm (standard deviation) from 50 TEM measurements. The particle concentration was measured to be 1.8×10^{13} ml^{-1} by extinction spectroscopy.[29] pNIPAM was coupled to the particle surface by ligand exchange: 4 ml of a 0.1 mg/ml aqueous solution of amine-terminated pNIPAM (5.5 kDa, Sigma) was added to 32 ml of the AuNP suspension. This mixture was heated to 40°C and 4 ml of a 1 mg/ml solution of the pNIPAM was added. The purpose of this procedure is to add the pNIPAM ligand in the hot (collapsed) state in order to optimize the packing density so that there is space for the expansion and collapse of each molecule. The resulting suspension was cooled to room temperature to give Au@pNIPAM core-shell nanoparticles. These particles were concentrated by centrifugation and resuspended in the supernatant to 10^{14} ml^{-1}, with the concentration measured from the extinction through the microdroplets.

Microfluidics

Poly(dimethylsiloxane) (PDMS) microfluidic devices were prepared by a standard soft lithography procedure. In summary, PDMS was cast onto an SU-8 master and cured at 70°C. The PDMS was then removed from the master, 1.0 mm holes were punched for the inlets/outlets and then the PDMS was plasma bonded to glass slides. The channels were functionalized with fluorocarbon using trichloro(1H,1H,2H,2H-perfluorooctyl)silane (Alfa Aesar, 0.5% v/v in FC40). Flow was driven using syringe pumps (New Era NE-1000). For microdroplet generation NOVEC 7500 with 0.5 wt% Pico-Surf 1 (Sphere Fluidics) was used as the oil phase and the concentrated Au@pNIPAM nanoparticle suspension was used as the aqueous phase.

Microscopy

Microscopy and microspectroscopy were performed using a modified Olympus BX-51 equipped with a Linkam hotstage. Optical heating is carried out using a 447 nm laser fiber-coupled into the microscope. Spectra were taken from microscopic regions by fiber coupling a spectrometer (Ocean Optics QEPro) in a conjugate image plane, with a long-pass filter to exclude the laser light. For capturing the ballistic droplet movement, a high speed camera was used (Photron Fastcam UX50).

Supporting Information

Supporting Information is available from the Wiley Online Library or from the author.

Acknowledgements

The authors acknowledge the support from EPSRC grants EP/N016920/1 and EP/L027151/1, and ERC grants LINASS 320503 and ANTNAM 77861E. S. C. acknowledges support of the Winton Programme for the Physics of Sustainability.

Received: ((will be filled in by the editorial staff))
Revised: ((will be filled in by the editorial staff))
Published online: ((will be filled in by the editorial staff))

References

[1] J. B. Messenger, *Biol. Rev. Camb. Philos. Soc.* **2001**, *76*, 473.
[2] R. C. Duarte, A. A. V. Flores, M. Stevens, *Philos. Trans. R. Soc. B Biol. Sci.* **2017**, *372*, DOI 10.1098/rstb.2016.0342.
[3] T. L. Williams, S. L. Senft, J. Yeo, F. J. Martín-Martínez, A. M. Kuzirian, C. A. Martin, C. W. DiBona, C. T. Chen, S. R. Dinneen, H. T. Nguyen, C. M. Gomes, J. J. C. Rosenthal, M. D. MacManes, F. Chu, M. J. Buehler, R. T. Hanlon, L. F. Deravi, *Nat. Commun.* **2019**, *10*, 1.
[4] S. Aoyama, M. Shimoike, Y. Hiratsuka, *Proc. Natl. Acad. Sci.* **2013**, *110*, 16408.
[5] C. Yu, Y. Li, X. Zhang, X. Huang, V. Malyarchuk, S. Wang, Y. Shi, L. Gao, Y. Su, Y. Zhang, H. Xu, R. T. Hanlon, Y. Huang, J. A. Rogers, *Proc. Natl. Acad. Sci.* **2014**, *111*, 12998.
[6] S. A. Morin, R. F. Shepherd, S. W. Kwok, A. A. Stokes, A. Nemiroski, G. M. Whitesides, *Science (80-.).* **2012**, *337*, 828.
[7] Q. Wang, G. R. Gossweiler, S. L. Craig, X. Zhao, *Nat. Commun.* **2014**, *5*, 1.
[8] S. Palagi, A. G. Mark, S. Y. Reigh, K. Melde, T. Qiu, H. Zeng, C. Parmeggiani, D. Martella, A. Sanchez-Castillo, N. Kapernaum, F. Giesselmann, D. S. Wiersma, E. Lauga, P. Fischer, *Nat. Mater.* **2016**, *15*, 647.
[9] B. Dai, J. Wang, Z. Xiong, X. Zhan, W. Dai, C. C. Li, S. P. Feng, J. Tang, *Nat. Nanotechnol.* **2016**, *11*, 1087.
[10] H.-W. Huang, F. E. Uslu, P. Katsamba, E. Lauga, M. S. Sakar, B. J. Nelson, *Sci. Adv.* **2019**, *5*, eaau1532.
[11] L. Xu, F. Mou, H. Gong, M. Luo, J. Guan, *Chem. Soc. Rev.* **2017**, *46*, 6905.
[12] F. Schmidt, B. Liebchen, H. Löwen, G. Volpe, *J. Chem. Phys.* **2019**, *150*, DOI 10.1063/1.5079861.
[13] T. Ding, V. K. Valev, A. R. Salmon, C. J. Forman, S. K. Smoukov, O. A. Scherman, D. Frenkel, J. J. Baumberg, *Proc. Natl. Acad. Sci.* **2016**, *113*, 5503.
[14] V. A. Turek, S. Cormier, B. Sierra-Martin, U. F. Keyser, T. Ding, J. J. Baumberg, *Adv. Opt. Mater.* **2018**, *6*, 1.
[15] Y. Liu, X. Dai, S. Mallawaarachchi, H. Hapuarachchi, Q. Shi, D. Dong, S. H. Thang, M. Premaratne, W. Cheng, *J. Mater. Chem. C* **2017**, *5*, 10926.
[16] J. Shen, B. Luan, H. Pei, Z. Yang, X. Zuo, G. Liu, J. Shi, L. Wang, R. Zhou, W. Cheng, C. Fan, *Adv. Mater.* **2017**, *29*, 1.
[17] M. Y. Lin, H. M. Lindsay, D. A. Weitz, R. Klein, R. C. Ball, P. Meakin, *J. Phys. Condens. Matter* **1990**, *2*, 3093.
[18] R. Esteban, R. W. Taylor, J. J. Baumberg, J. Aizpurua, *Langmuir* **2012**, *28*, 8881.
[19] D. W. Logan, S. F. Burn, I. J. Jackson, *Pigment Cell Res.* **2006**, *19*, 206.
[20] S. M. Sohel Murshed, *Electronics Cooling*, Intech, Rijeka, **2016**.
[21] A. R. Salmon, R. Esteban, R. W. Taylor, J. T. Hugall, C. A. Smith, G. Whyte, O. A. Scherman, J. Aizpurua, C. Abell, J. J. Baumberg, *Small* **2016**, *12*, 1788.
[22] Z. Li, W. Richtering, T. Ngai, *Soft Matter* **2014**, *10*, 6182.
[23] C. Monteux, C. Marliére, P. Paris, N. Pantoustier, N. Sanson, P. Perrin, *Langmuir* **2010**, *26*, 13839.
[24] E. M. Purcell, *Am. J. Phys.* **1977**, *45*, 3.
[25] S. Herminghaus, C. C. Maass, C. Krüger, S. Thutupalli, L. Goehring, C. Bahr, *Soft Matter* **2014**, *10*, 7008.
[26] S. Cormier, T. Ding, V. Turek, J. J. Baumberg, *Adv. Opt. Mater.* **2018**, *6*, 1.
[27] R. Battino, T. R. Rettich, T. Tominaga, *J. Phys. Chem. Ref. Data* **1984**, *13*, 563.
[28] C. Li, D. Li, G. Wan, J. Xu, W. Hou, *Nanoscale Res. Lett.* **2011**, *6*, 440.

[29] W. Haiss, N. T. K. Thanh, J. Aveyard, D. G. Fernig, *Anal. Chem.* **2007**, *79*, 4215.